Fundamental relation between wave fields, rocking curves, and anomalous absorption for the reflection high-energy electron diffraction of Si(111) crystals

Yoshimi Horio
Department of Applied Electronics, Daido Institute of Technology, 2-21 Daido-cho, Minami-ku, Nagoya 457, Japan
(Received 14 July 1997; revised manuscript received 8 September 1997)

Based on a dynamical theory of electron diffraction, electron wave fields close to the crystal surface as well as reflection high-energy electron diffraction rocking curves are calculated for the Si(111) surface at $[\bar{1}\,1\,2]$ incidence. The following five cases are considered: single layer, one bilayer, two-bilayer, three-bilayer, and semi-infinite thickness of Si(111) crystal with bulk truncated surface. The rocking curves of the total intensity of all the reflected and transmitted electron beams show two minima corresponding to surface wave resonance conditions except for the single-layer case. These characteristic minima of the total intensity suggest the existence of anomalous absorption of incident beam in the Si(111) crystal. It is established that at the positions of these minima the calculated intensity of the wave field on Si atomic rows increases and furtheremore Auger electron intensity of Si(LVV) emitted from the surface is enhanced. [S0163-1829(98)00508-6]

I. INTRODUCTION

In a reflection high-energy electron diffraction (RHEED) study,[1,2] diffraction patterns or diffraction spot intensities give information on surface atomic structure. For example, an experimentally obtained glancing angle dependence of diffraction spot intensity, the rocking curve, is used for the determination of a surface atomic structure by comparison with a calculated rocking curve.[3–6] The oscillation of a diffraction spot intensity during the growth of a thin film on a substrate crystal, the RHEED oscillation, is useful for growth mode study of thin films at several growth conditions.[7–12]

An investigation of the electron wave field, which is constructed in a crystal surface region by interference among several plane waves of incident and diffracted electrons in RHEED conditions is useful in several aspects as follows. (1) Peaks in a rocking curve regularly appear at Bragg reflection angles provided that the one-beam condition[13,14] is satisfied, where the azimuth of the incident beam direction is slightly turned away from a certain crystallographic direction in order to avoid simultaneous reflections. Generally, the profile of a rocking curve is complicated by the precise crystallographic direction of the incident beam. In this case, a wave field consideration is helpful in clarifying the origins of peaks in a rocking curve. (2) Secondary electrons, especially Auger electrons[15–20] and characteristic x rays[21–24] are excited and emitted from the surface during RHEED experiments. These Auger electrons and/or x rays also give information on surface structures by relating their intensities to the wave fields formed in a crystal surface region,[25] because these excitations are enhanced when the wave field concentrates on atomic rows. For the purpose of the complementary method of surface structure analysis, it is important to study the behavior of wave fields at a crystal surface region upon changing the incident beam condition. (3) Wave fields are also necessary in considering inelastic scattering problems dependent on the channeling paths of incident electrons in a crystal.[26] (4) There is the possibility of a novel technique whereby an intense electron wave field could carve a certain periodic pattern on a thin crystal film surface on a nanoscale or carry out a selective excitation on different atomic rows.

With regard to these, preliminary calculations have already been carried out of wave fields in Si(111) layers together with rocking curves for the diffraction beams.[27] However, the calculations did not take into account the absorption effects of electrons in the crystal. This was because the treated crystals were extremely thin, that is less than a few bilayers, and accordingly only the fundamental relationship between the behavior of the wave field and the rocking curve was focused on. The calculated results did though give important information on the origins of peaks in the rocking curves.

In this paper, the calculations of wave fields and rocking curves are improved so that imaginary crystal (scattering) potential is included and the absorption effect is discussed. Furtheremore, the crystal potential is corrected to a more realistic value. The treated crystal is not only a few Si(111) bilayer cases but also more realistic semi-infinite Si(111) cases. Calculated rocking curves excluding and including ab-

TABLE I. Diffraction conditions.

Reflection index	Glancing angle (deg)[a]
222	1.00
333	2.69
SWR (due to 11 and $\bar{1}\,\bar{1}$ ros)[b]	3.05
402 and 042	3.14
$3\,\bar{1}\,1$ and $\bar{1}31$	3.57
Emergences of 11 and $\bar{1}\,\bar{1}$ beams[c]	3.64
513 and 153	3.85
444	3.99
624 and 264	4.81
555	5.21
735 and 375	5.85

[a]Estimated by using $V_{000}=12$ eV.
[b]Internal emergence threshold (IT).
[c]Vacuum emergence threshold (VT).

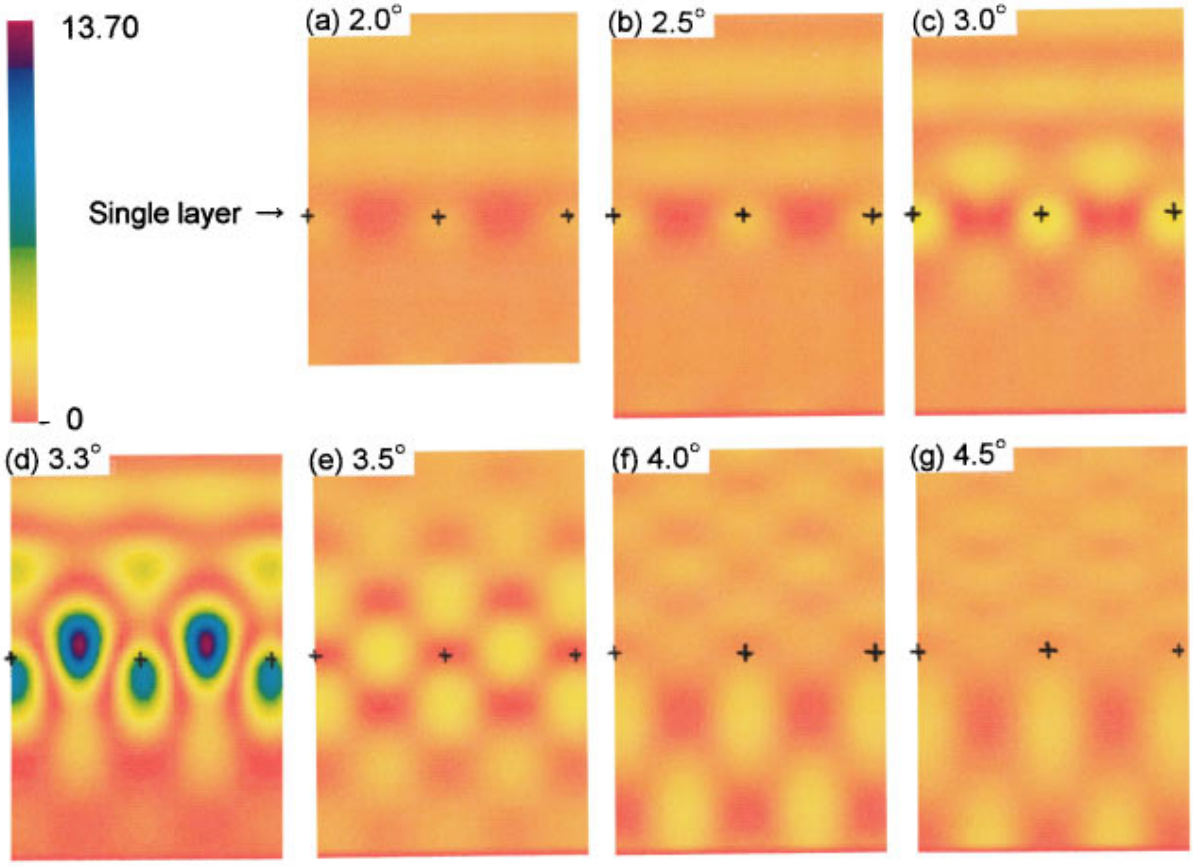

FIG. 1. (Color) Wave fields for the single-layer case at various glancing angles.

sorption effect are compared with each other and the differences are discussed. Especially, the relation between the amount of absorption of the incident electron beam in the crystal and the Auger electron intensity emitted from the crystal surface upon changing the glancing angle is investigated.

II. CALCULATIONS

Wave fields in a crystal are calculated by using the multislice method[4,28] of dynamical theory of electron diffraction. The term ''wave field'' means the spatial distribution of the intensity of the electron wave function formed in a crystal (or out of a crystal) by an incident high-energy electron beam and the resulting diffracted electron beams. Three reciprocal rods (00, 11, and $\overline{1\,1}$) are taken into account in the calculations. The acceleration voltage of the incident electron beam is set at 10 kV. The direction of the incident beam is fixed at the $[\overline{1}\,12]$ azimuth. Wave fields are calculated in a plane perpendicular to the $[\overline{1}\,12]$ direction for various incident glancing angles. There is no modulation of the wave field along the $[\overline{1}\,12]$ direction, because only beams in the zeroth Laue zone are taken into account in the calculations.

Four crystal cases of Si(111) (Ref. 27) such as single layer, one bilayer, two-bilayer, and three-bilayer, are treated together with the more realistic case of the Si(111) crystal with semi-infinite thickness. For the semi-infinite crystal case, 33 bilayers ($\sim$100 Å thickness) are actually taken into account in the calculation and the number of bilayers is sufficient for numerical convergence due to absorption. The crystal potentials (or scattering potentials) are calculated from the tabulation of Doyle and Turner[29] and the mean inner potential V_{000} of the bulk Si is deduced as 13.9 V. This value is slightly different from our previously obtained one of 12.0 ± 0.5 V (Ref. 13) by the comparison between the experimental rocking curve and the calculated one. The crystal potential of Si used in the calculations is corrected so that the mean inner potential V_{000} is set at 12 V. This is slightly different from the previous paper,[27] which used uncorrected potential. Calculations have been carried out by the multislice method[4,28] and every slice width is set at 0.1 Å. In the strict sense, Fourier coefficients of the imaginary potential that express absorption effects should be physically meaningful ones[30] especially in such a case as a structure determination. In this work, however, the imaginary part is simply assumed to be 10% of the real part because of focusing on the fundamental behaviors of absorption effects.

III. CALCULATED RESULTS AND DISCUSSIONS

Table I shows the glancing angles corresponding to several diffraction conditions. The values are estimated by using a mean inner potential V_{000} of 12 V. It should be noticed that the Ewald sphere comes in contact with both 11 and $\overline{1\,1}$ rods at $\theta=3.05°$. This condition is called the surface wave resonance (SWR) condition.[31,32] In practice, the glancing angles of the SWR conditions are related to the Bloch states.[33] Recently the detailed resonance scattering has been

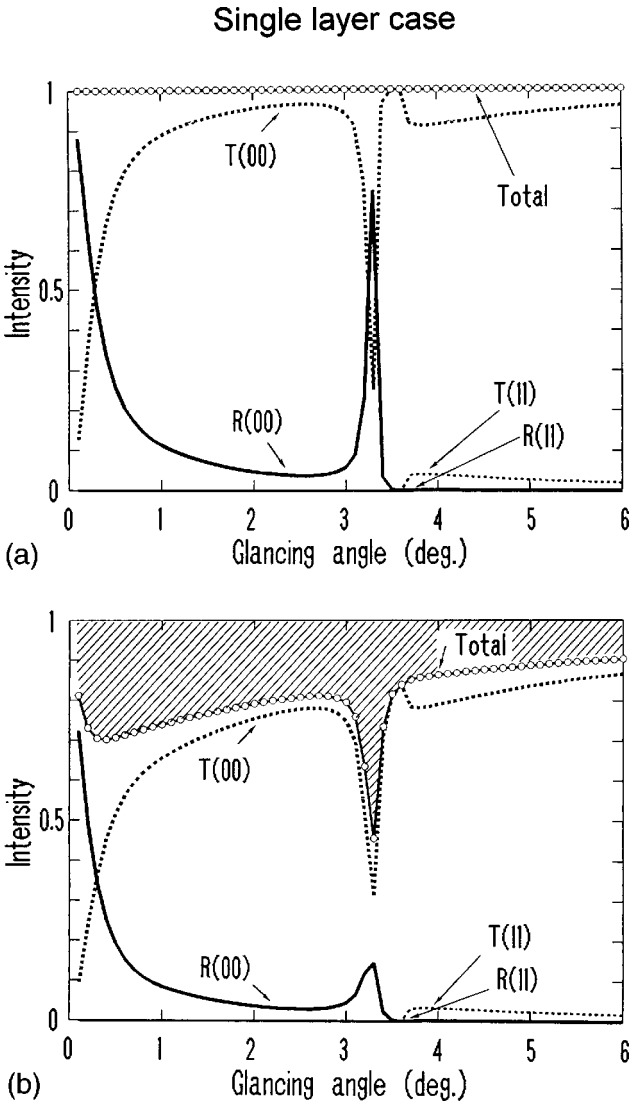

FIG. 2. Rocking curves for the single-layer case, where (a) and (b) show the calculated results without and with absorption effect, respectively. $R(00)$ and $T(00)$ indicate the intensities of the reflected and transmitted beams due to 00 rod, respectively. $R(11)$ [or $R(\overline{1\,1})$] and $T(11)$ [or $T(\overline{1\,1})$] indicate the intensities of the reflected and transmitted side beams due to the 11 (or $\overline{1\,1}$) rod, respectively. The shaded area denotes the amount of absorption, which is the difference between the incident beam intensity (unity) and the total intensity of the diffracted beams.

rigorously investigated by Dudarev and Whelan.[34,35] The energy levels and the number of Bloch states depend on the shape of the crystal potential such as the depth and the width. Therefore it is possible that the glancing angles of the SWR conditions are slightly different from the simply predicted angles in Table I by using only the mean inner potential. At the SWR condition, excited side beams due to the 11 and $\overline{1\,1}$ rods run almost parallel to the surface and can emerge into the vacuum for $\theta > 3.64°$.

Calculated wave fields as shown in the following subsections all take into account absorption effects. The wave fields are mapped by color scale and all maps are normalized by their maximum value for every crystal case. The method of normalization is different from Ref. 27, where each map was normalized by each maximum value. Therefore we can compare the absolute intensities of wave fields at different glancing angles to each other for a particular crystal case. Purple regions indicate higher intensities than red regions. It should be noted that since the calculated wave fields are obtained by the square of the absolute intensities of electron wave functions, the phases of the electron wave functions are extinguished. The symbols ''+'' indicate the positions of the atomic rows of Si along the $[\overline{1\,1\,2}]$ direction (perpendicular to the paper), which are arrayed laterally with the interval of $d_{220}=1.92$ Å and vertically with the main interval of $d_{111}=3.14$ Å and the subinterval of $d_{444}=0.78$ Å.

A. Single-layer case

Calculated wave fields for the single layer are shown in Fig. 1. At lower glancing angles such as $\theta \lesssim 2.5°$, wave fields show simple forms. Wave field intensity on atomic rows (indicated by symbol ''+'') is usually stronger than that on interatomic rows at such low angles. This feature is also commonly seen in the other cases of the following subsections. Standing waves seen in the vacuum above the crystal are due to the interference between the incident beam and the specularly reflected beam. At about $\theta \gtrsim 2.5°$, the wave field begins to be modulated laterally . The wave field intensity has a maximum at $\theta = 3.3°$ due to SWR of the 11 and $\overline{1\,1}$ side beams. The laterally modulated intense wave field is formed by the intereference of these side beams running parallel to the surface. This glancing angle is 0.25° higher than that in Table I. It is mainly due to the slightly shallower potential depth in the single layer case compared with those of the other cases. This is because there are no neighboring layers and no contributions to the single-layer potential from the others. At this SWR condition, the intensity of the wave field has maxima not only at atomic rows but also at interatomic rows, and the latter is stronger than the former. For $3.3° \lesssim \theta \lesssim 3.6°$, the side beams due to the 11 and $\overline{1\,1}$ rods are excited in the crystal but they can not emerge into the vacuum because of the potential barrier. Consequently, wave fields in the crystal are modulated by these side beams. For $\theta \gtrsim 3.6°$, the side beams emerge into the vacuum mostly as transmission beams rather than reflection beams because of the high transmissivity due to the extremely thin layer case.

Rocking curves of the reflected and transmitted beams of the 00, 11, and $\overline{1\,1}$ rods are shown in Fig. 2. Solid and dotted lines indicate the rocking curves of the reflected and transmitted beams, respectively. Figure 2(a) shows calculated results without the absorption effect, similar to Ref. 27, and Fig. 2(b) with the absorption effect. $R(00)$ and $R(11)$ denote the reflected beams of the 00 and 11 rods, respectively, and $T(00)$ and $T(11)$ the transmitted beams of the 00 and 11 rods, respectively. Since $R(\overline{1\,1})$ [or $T(\overline{1\,1})$] has the same intensity as $R(11)$ [or $T(11)$] at the symmetric condition of such $[\overline{1\,1\,2}]$ incidence, the rocking curve of $R(\overline{1\,1})$ [or $T(\overline{1\,1})$] is omitted from the figures. Small open circles in the figures indicate the total intensity of the reflected beams [$R(00)$, $R(11)$, and $R(\overline{1\,1})$] and the transmitted beams [$T(00)$, $T(11)$, and $T(\overline{1\,1})$]. The difference between the total intensity and the incident beam intensity which is taken as

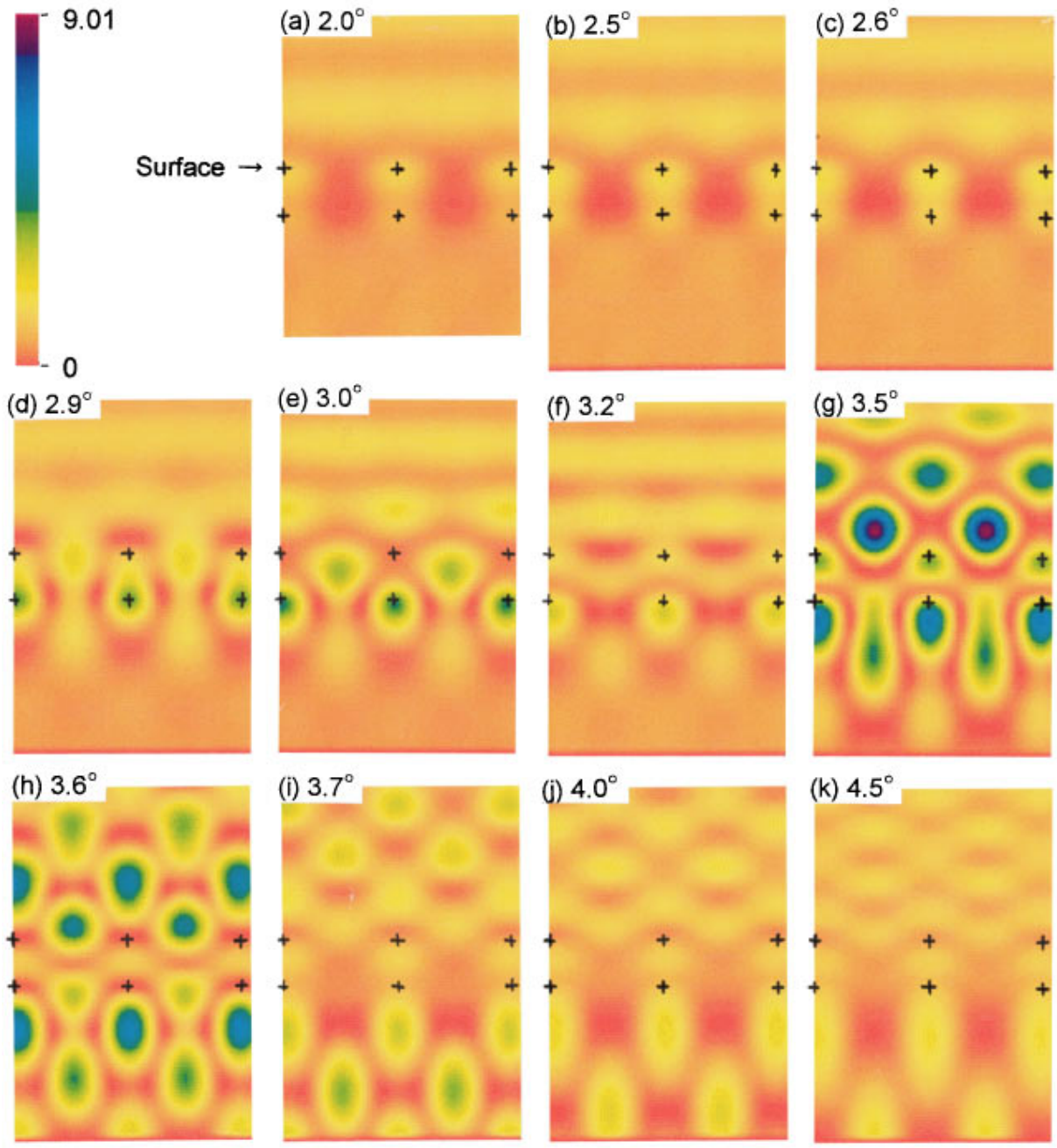

FIG. 3. (Color) Wave fields for the one-bilayer case.

unity, corresponds to the amount of absorption of incident beam in the crystal. The amount of absorption is shown by the shaded area in Fig. 2(b).

The rocking curve of each beam shows a very simple profile especially in this single-layer case. Only a single peak (or single dip) appears in the $R(00)$ [or $T(00)$] rocking curve at $\theta=3.3°$. In Fig. 2(a), the total intensity shows a constant value of unity for changing glancing angle. That is, the total intensity of the diffracted electron beams always equals the intensity of the incident electron beam, because there is no absorption of incident beam in the crystal. On the other hand, it is found in Fig. 2(b) that the total intensity shows an anomalous behavior at the SWR condition of $\theta=3.3°$, which just corresponds to a peak (or a dip) position in the rocking curve of the specular beam $R(00)$ [or direct beam $T(00)$].

The single sharp peak of $R(00)$ at $\theta=3.3°$ in Fig. 2(a) decreases in intensity as shown in Fig. 2(b) due to absorption. The reason is considered as follows. At $\theta=3.3°$, the wave field concentrates intensely on both atomic and interatomic rows as shown in Fig. 1(d). The electrons constructing the intense wave field run parallel to the surface and then contribute to the intensity of specular reflection beam $R(00)$ according to the reciprocity theorem. In the case of Fig. 2(b), electrons passing through atomic rows especially suffer strong absorption and weaken. This makes the intensity of the $R(00)$ weak.

The 11 and $\overline{1}\,1$ side beams begin to appear at the emergence angle of 3.64°, but their intensities are very weak. When the number of atomic layers is increased, the wave

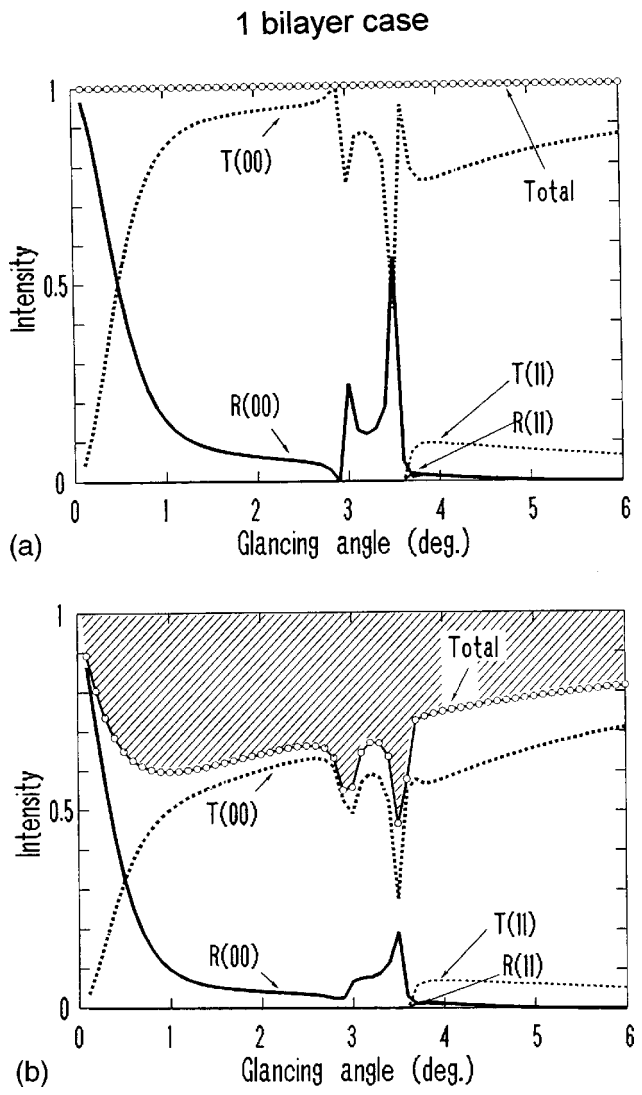

FIG. 4. Rocking curves for the one-bilayer case.

fields are modulated compared to those in the single-layer case and the rocking curves contain more complicated peaks.

B. One-bilayer case

Figure 3 shows the wave fields for the one-bilayer case. The behavior of the wave fields is generally similar to those in the single-layer case, however, the following point is different. Upon changing the glancing angle, highly localized wave fields appear twice, around $\theta=3.0°$ and around 3.5°, and both are considered to be due to the SWR of the 11 and $\overline{1}\,1$ rods. At $\theta=3.0°$, the wave field concentrates on the atomic rows in the lower layer of the bilayer, but not so on the atomic layer in the upper layer. Furthermore, the wave field intensity concentrates on the interatomic rows (the z position is located around the middle of the bilayer). The pattern of the wave field is similar to that in Fig. 1(d) of the single-layer case. The SWR condition at 3.0° is very close to the value of 3.05° in Table I, which is called the ''internal emergence threshold (IT)'' of the side beams. At $\theta=3.5°$, on the other hand, the wave field concentrates on the atomic rows in both upper and lower layers of the bilayer. Furthermore, the wave field intensely concentrates on the interatomic rows (the z position is located slightly over the upper layer of the bilayer). This angle of 3.5° corresponds to just before the emergence angle 3.64° of the 11 and $\overline{1}\,1$ side beams into the vacuum, which is called as the ''vacuum emergence threshold (VT)'' of the side beams. At $\theta=3.6°$, the pattern of the wave field seems to be nearly symmetrical about the middle plane in the bilayer.

Figure 4 shows the rocking curves for the one-bilayer case. In Fig. 4(a), the rocking curve of $R(00)$ shows two intense peaks at $\theta=3.0°$ and $\theta=3.5°$, which just correspond to the formation of the highly localized wave fields descrived above. On the contrary, the rocking curve of $T(00)$ shows two sharp dips at the same glancing angles. The rocking curve of the total intensity is constant because there is no absorption. In Fig. 4(b), the rocking curve of the total intensity shows two dips due to the absorption effect and the profile is similar to that of the $T(00)$ rocking curve. The two sharp peaks of the $R(00)$ rocking curve in Fig. 4(a) decrease in intensity as shown in Fig. 4(b). The two peaks seem to be a separation of the single peak at $\theta=3.3°$ in the single-layer case. It may be considered as a Bloch state in the crystal potential of the single-layer case being separated into two Bloch states (two energy levels) by adding one more single layer potential at the close distance of $d_{444}=0.78$ Å . The deeper and shallower Bloch states nearly correspond to the internal and vacuum emergence thresholds of the side beams, respectively. The two Bloch states are the fundamental feature of the Si(111) crystal as shown in the following cases. The rocking curve of the 11 side beam becomes slightly stronger than that for the single-layer case, but is still monotonous.

C. Two-bilayer case

Figure 5 shows the wave fields for the two-bilayer case, where an interbilayer distance d_{111} (3.14 Å) exists. Around $\theta=2.6°$, a standing wave appears with three nodes in the region between the first and the second bilayers, which is considered to be caused by the 333 reflection. At $\theta=3.0°$ as shown in Fig. 5(c), the wave field intensely concentrates on the first bilayer as in Fig. 3(e) of the one-bilayer case and a similar pattern of the wave field also weakly appears on the second bilayer. At $\theta=3.5°$ of Fig. 5(e), the wave field concentrates on all the atomic rows in both the first and the second bilayers and more intensely on the interatomic rows, with locations slightly over the first and the third layers. The wave field at the first (or the second) bilayer is similar to Fig. 3(g) of the one-bilayer case. At the middle planes in the first (or the second) bilayer, the wave field intensity is especially very weak. For these glancing angles of $3.0°-3.5°$, the wave fields in the crystal are sensitively influenced by the four evanescent beams (two reflection beams and two transmission ones due to 11 and $\overline{1}\,1$ rods). For $\theta>3.6°$, the 11 and $\overline{1}\,1$ side beams can emerge into vacuum.

Figure 6 shows the rocking curves for the two-bilayer case. In Fig. 6(a), the characteristic feature of the $R(00)$ rocking curve is the narrow split of the peak at $\theta=3.5°$ in the one bilayer case into peaks at 3.4° and 3.6°. The narrow split is considered to be caused by a narrow split of a Bloch state, which arises from a weak interaction between the two bilay-

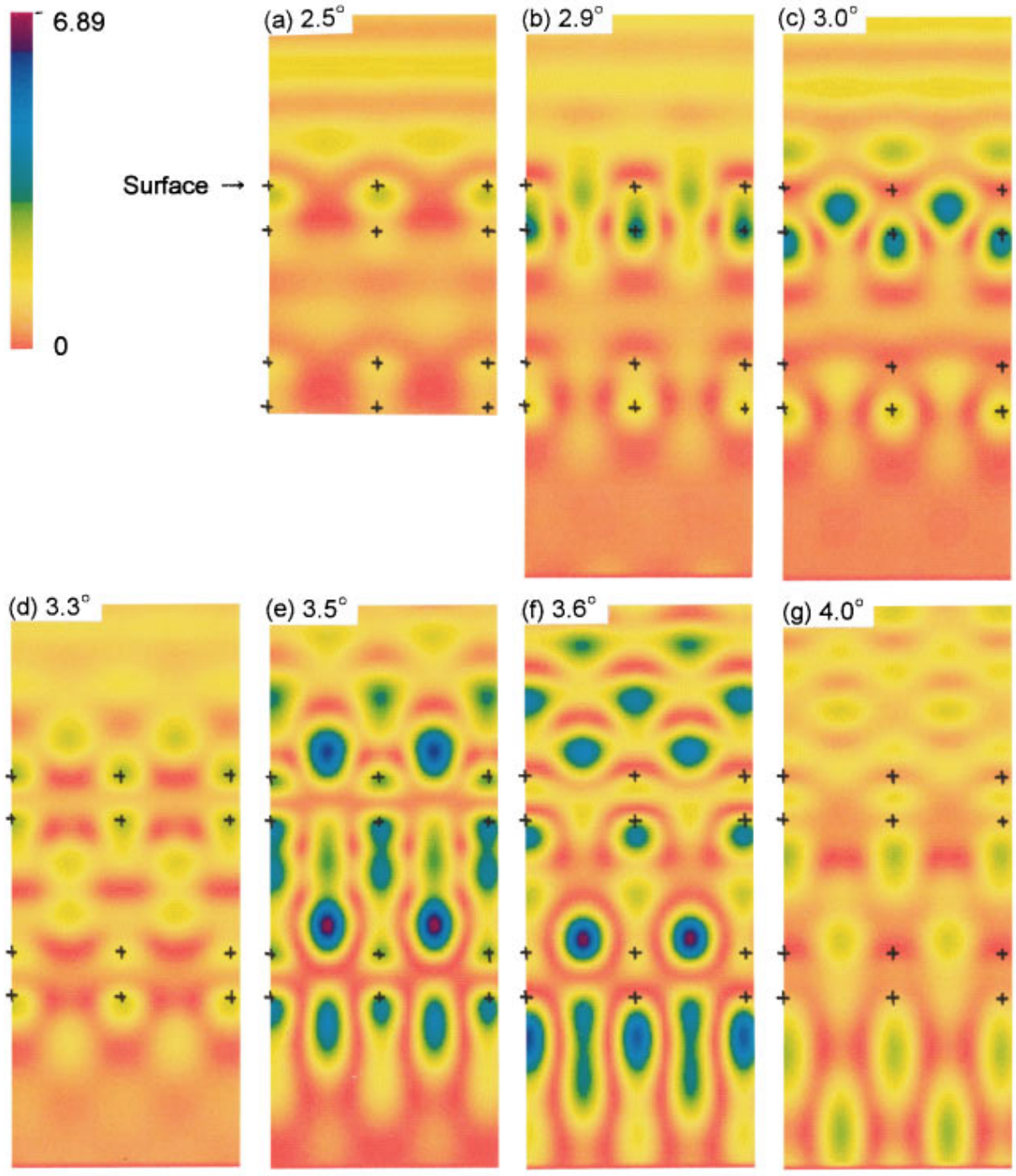

FIG. 5. (Color) Wave fields for the two-bilayer case.

ers with $d_{111}=3.14$ Å apart from each other. A new broad peak appears around $\theta=2.6°$. The broad peak is considered to be the 333 Bragg reflection because of the wave field consideration described above. The two sharp peaks of Fig. 6(a) at $\theta=3.0°$ and 3.6° become weak and comparable to the broad 333 peak as shown in Fig. 6(b). It is considered that the two peaks are strongly influenced by the absorption effect. At the same time, the total intensity also decreases at $\theta=3.0°$ and 3.5°, which means that the absorption increases at these glancing angles; that is, the wave field intensities on the atomic rows increase as a whole. The intensity of the $R(11)$ [or $R(\overline{1}\,\overline{1})$] reflection beam increases compared with that for the one bilayer case.

D. Three-bilayer case

Figure 7 shows the wave fields for three-bilayer case. The fundamental behavior of the wave field is similar to that for the two-bilayer case. At $\theta=3.0°$ as shown in Fig. 7(b), the wave field is very highly concentrated on the first bilayer.

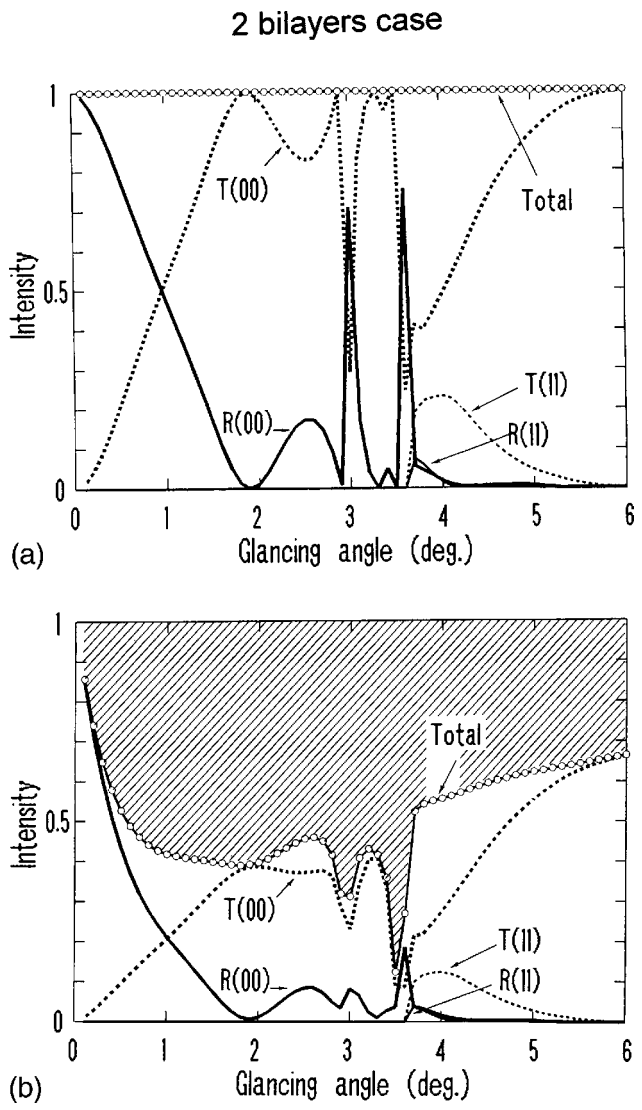

FIG. 6. Rocking curves for the two-bilayer case.

The concentration on the first bilayer is similar to those for one-bilayer and the two-bilayer cases. The next high concentration of the wave field appears around $\theta=3.5°–3.6°$ and the features of the wave field are also similar to those for the one-bilayer and the two-bilayer cases. The wave field concentrates not only on each atomic row in each bilayer but also intensely on each interatomic row.

Figure 8 shows the rocking curves for the three-bilayer case. For the $R(00)$ rocking curve in Fig. 8(a), a very intense peak appears at the same angle of 3.0° as for the two-bilayer case, however, it is accompanied by a small peak at $\theta=1.9°$. The sharp peak at $\theta=3.5°$ in the one-bilayer case seems to be split into two peaks at $\theta=3.3°$ and 3.7°, which is a wider separation than the two-bilayer case. The strong peak at $\theta=3.0°$ becomes very small when absorption is included as shown in Fig. 8(b). The fundamental features of the total intensity curve are similar to the one-bilayer case; that is, it shows two dips around $\theta=3.0°$ and 3.6°. The $R(11)$ [or $R(\overline{1\,1})$] rocking curve has only a small amount of structure.

E. Semi-infinite crystal case

The wave fields and the rocking curves were also calculated for the semi-infinite crystal case of Si(111) as shown in Fig. 9 and Fig. 10, respectively. In Fig. 9, the wave fields are shown around the top three bilayers. The crystal surface is treated as a bulk truncated 1×1 structure. The absorption effect is taken into account in these calculations. It is seen by comparing the wave fields in Figs. 7 and 9 and also comparing the rocking curves in Figs. 8(b) and 10 that the behavior of the wave fields and the rocking curves for this case is rather similar to that for the three-bilayer case. The main peaks of $R(00)$ at $\theta=2.6°$, 3.0°, and 3.7° in Fig. 10 agree well with those of the three-bilayer case in Fig. 8(b). Therefore it is considered that a three-bilayer thickness is the effective depth region of RHEED with a 10-kV incident beam.

In the higher glancing angle region $\theta\gtrsim5°$, however, the calculated peak intensities for the three-bilayer case are slightly weaker than those for the semi-infinite case, for example, as seen in the peak intensity at 4.8°. The reason is that a small part of the incident beam passes through the three-bilayer crystal in such a higher angle region and cannot contribute to the reflection intensities.

The calculated rocking curves of 00 and 11 beams in Fig. 10 are in relatively good agreement with experimental ones,[26] which were taken from the Si(111)7×7 surface, except for the glancing angle region smaller than about 2°. At such a low glancing angle region, rocking curves become very sensitive to the surface structure and big differences are recognized, because the calculated rocking curves are based on the bulk truncated 1×1 surface. However, at $\theta\gtrsim2°$, the calculated and experimental rocking curves agree relatively well.

IV. COMPARISON BETWEEN ANOMALOUS ABSORPTION AND AUGER INTENSITY

Figure 11 shows two curves. One is an absorption curve (open circles) for the incident electron in the crystal, which is obtained by the difference between unity (incident beam intensity) and the total intensity in Fig. 8(b) of the three-bilayer case. The other dotted curve shows the Auger intensity of Si(LVV) upon changing the glancing angle, BRAES (beam rocking Auger electron signal intensity) curve, which was taken from a Si(111)7×7 surface for the same incident conditions as the calculated one. It can be seen that the positions of the two peaks around $\theta=3.0°$ and 3.6° in the absorption curve are in good agreement with those of the two peaks in the BRAES curve. Accordingly the localization of wave field on atomic rows corresponds to the enhancement of the excitation of Si(LVV) Auger electrons.

As shown in Fig. 9(b), the wave field intensely concentrates on the atomic rows of the lower layer of the first bilayer at $\theta=3.0°$. Around $\theta=3.5°–3.6°$, the wave field concentrates on both atomic rows of the upper and lower layers of the first bilayer as shown in Figs. 9(d) and 9(e). These localized wave field intensities on atomic rows decrease with increasing depth.[36,37] The enhancement of Auger electron intensity is considered to be due to such wave field localization on atomic rows. At the same time the wave field localization

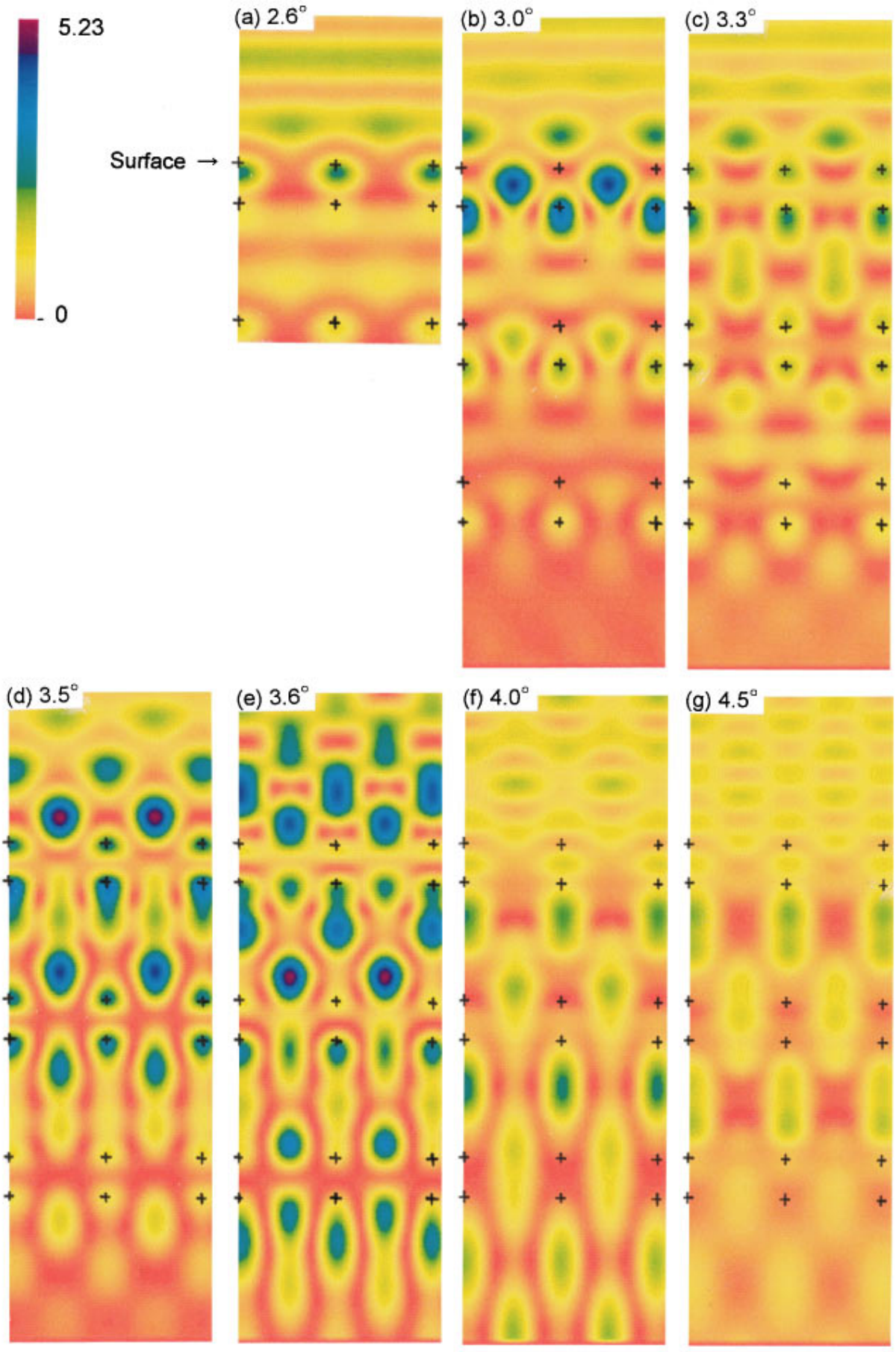

FIG. 7. (Color) Wave fields for the three-bilayer case.

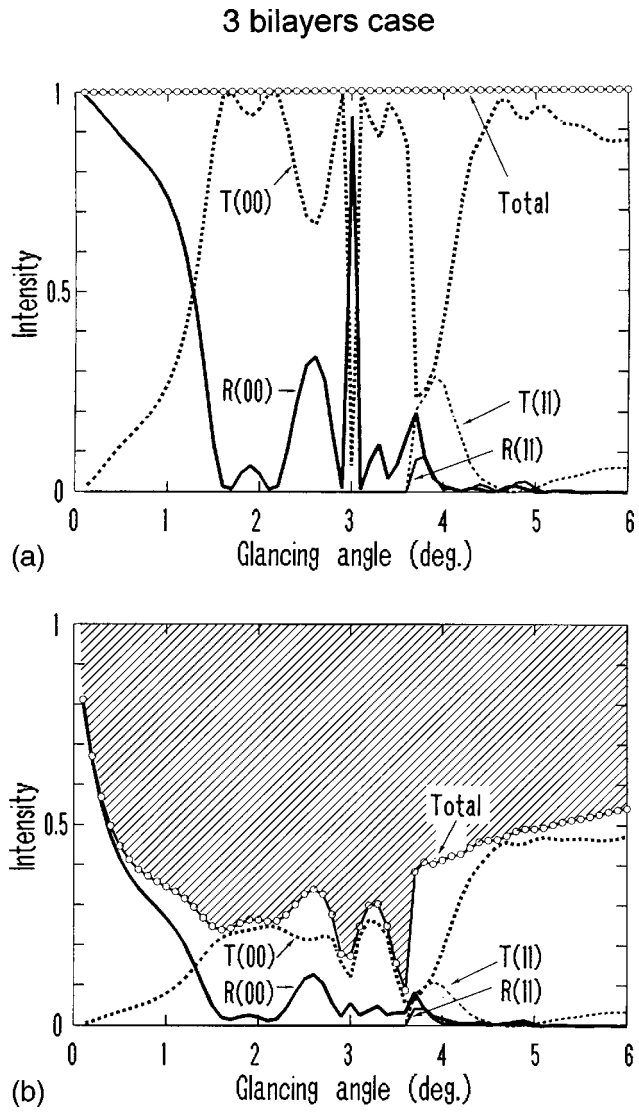

FIG. 8. Rocking curves for the three-bilayer case.

on atomic rows increases the absorption of incident electron beam. Considering the relatively good reproduction of the experimental rocking curves by the calculations for the three-bilayer or the semi-infinite crystal cases, calculated wave fields are also considered to represent rather realistic one in the region of $\theta \gtrsim 2°$.

V. SUMMARY

Wave fields and rocking curves have been calculated based on a dynamical theory of electron diffraction with three rods for 10-keV incident electron. The incident azimuth is fixed at the $[\overline{1}\,1\,2]$ direction, where the simultaneous reflections of the 11 and $\overline{1}\,1$ side beams occur, accompanied by dynamical effects. The crystals used for the calculations of the wave fields and the rocking curves are single layer, one bilayer, two-bilayer, three-bilayer, and semi-infinite cases of Si(111) with bulk truncated surface. In particular, absorption effects have been investigated by using total intensity curves of diffraction beams. The features of these calculated results for the several crystal cases are summarized as follows.

In the single-layer case, only one absorption peak appears at $\theta = 3.3°$. This reflects a Bloch state in the crystal potential for side beams and is due to a slightly shallow and narrow potential compared with those of the other cases with several bilayers.

In the one-bilayer case, two absorption peaks appear at $\theta = 3.0°$ and 3.5°. The wave field at $\theta = 3.0°$ is very similar to that of the single-layer case at $\theta = 3.3°$. The wave field on the atomic rows of the lower layer of the bilayer is intense and conversely that on the atomic rows of the upper layer is very weak. The wave field on the interatomic rows (the z position is located around the middle of the bilayer) is intense. On the other hand, at $\theta = 3.5°$, the wave field concentrates on the atomic rows of both the lower and the upper layers. Furthermore, the wave field is very intense slightly above the interatomic rows of the upper layer. It is considered that electrons passing through the interatomic rows near or above the surface construct such intense wave fields and contribute to the enhancement of the specular beam intensity according to the reciprocity theorem. On the other hand, electrons passing through atomic rows suffer strong aborption. The behavior for absorption effects and the wave field of the one-bilayer case is basically common to the other bilayers and semi-infinite cases.

The region from the top surface to the bottom of three bilayers is considered to be an effective depth in RHEED with 10-kV incident beam. Because the rocking curves and wave fields for the three-bilayer case are similar to those for the semi-infinite case, calculated rocking curves of 00 and 11 beams for the semi-infinite Si(111) crystal agree relatively well with the experimental results[26] taken from the Si(111)7×7 surface in the higher angle region of $\theta \gtrsim 2°$.

A calculated absorption curve of an incident electron beam and a experimental BRAES curve of Si(LVV) taken from a Si(111)7×7 surface were compared. It was found that the intensity anomalies of the Si(LVV) Auger electrons correspond to the calculated absorption peaks. The study of the relation between the intensity anomalies of Auger electrons and wave fields is now in progress for other surface structures. For a Si(111)$\sqrt{3}\times\sqrt{3}$-Al surface, reasonable result was obtained and will be described elsewhere.[38]

ACKNOWLEDGMENTS

Acknowledgments are made to Dr. A. E. Smith and Professor K. Mihama for their valuable advice. The present work has been supported by the Inamori Foundation and a Grant-in-Aid for Scientific Research (08455018) from the Ministry of Education, Science, Sports and Culture.

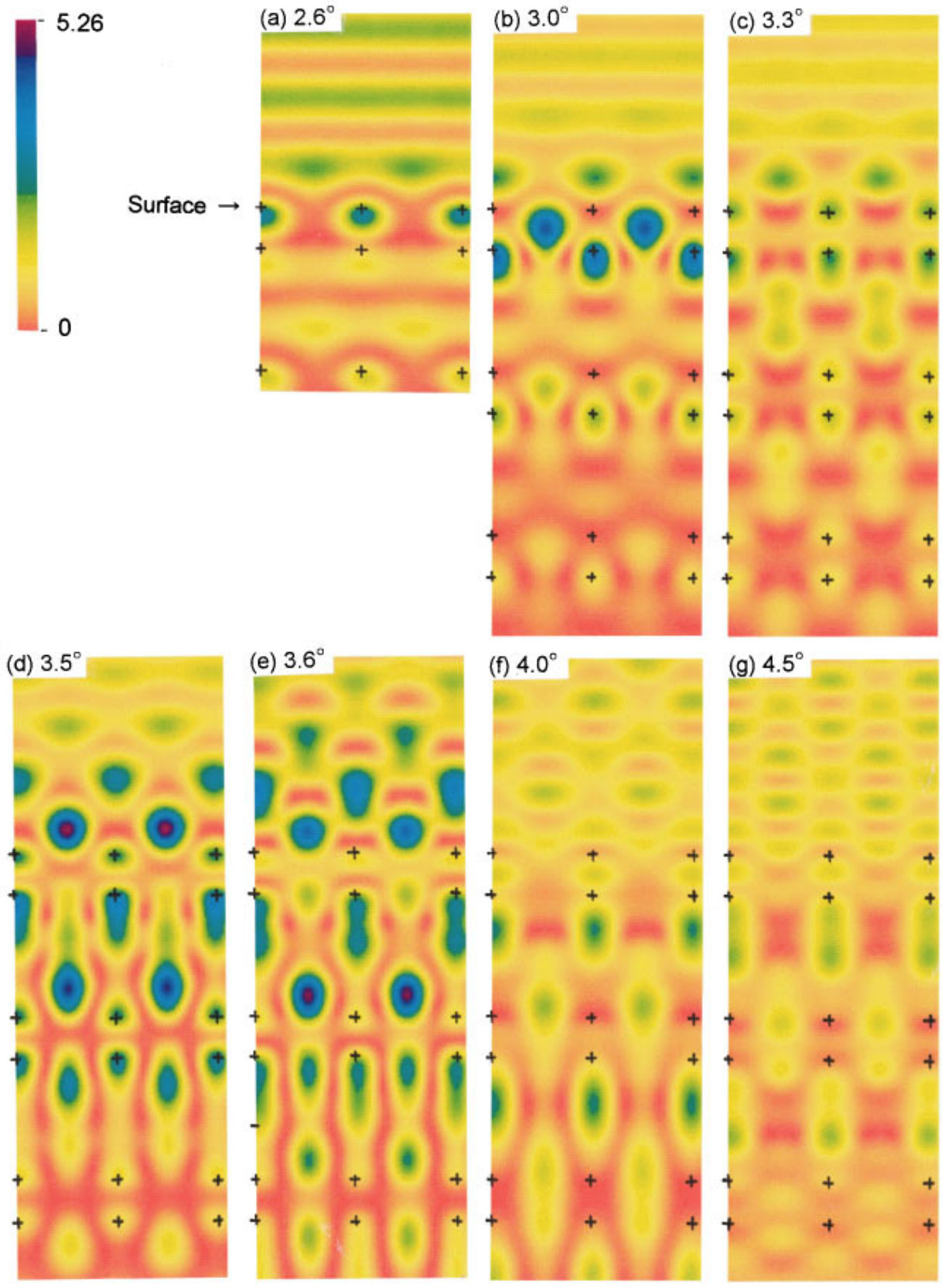

FIG. 9. (Color) Wave fields for the semi-infinite crystal case.

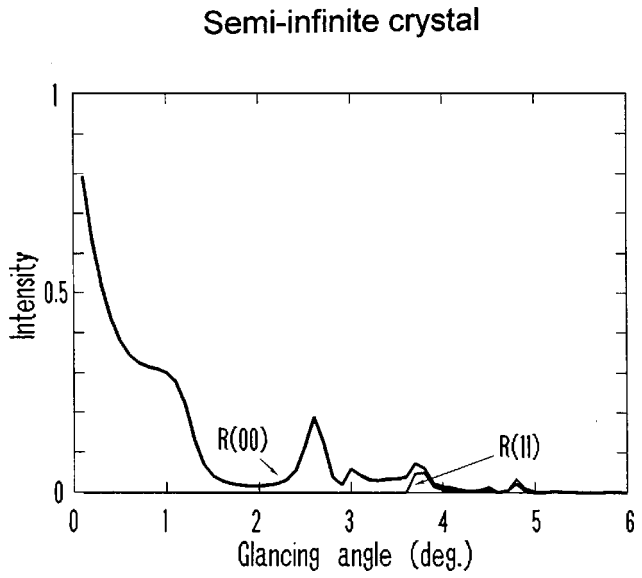

FIG. 10. Rocking curves for the semi-infinite crystal case.

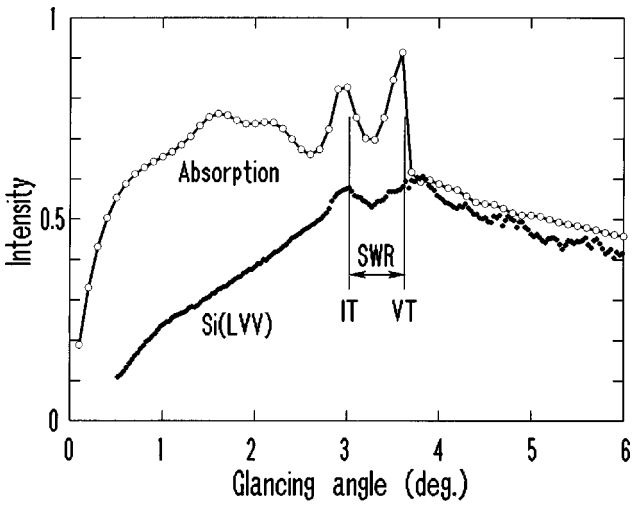

FIG. 11. Comparison between the absorption curve indicated by open circles and the BRAES curve of Si(LVV) indicated by dots.

[1] S. Miyake, Sci. Pap. Inst. Phys. Chem. Res. Tokyo. **26**, 216 (1935).
[2] S. Ino, Jpn. J. Appl. Phys. **16**, 891 (1977); **17**, 1121 (1978).
[3] T. C. Zhao and S. Y. Tong, Ultramicroscopy **26**, 151 (1988).
[4] A. Ichimiya, S. Kohmoto, T. Fujii, and Y. Horio, Appl. Surf. Sci. **41/42**, 82 (1989).
[5] T. Hanada, S. Ino, and H. Daimon, Surf. Sci. **313**, 143 (1994).
[6] Y. Horio, Surf. Rev. Lett. (to be published).
[7] J. J. Harris, B. A. Joyce, and P. J. Dobson, Surf. Sci. **139**, 121 (1984).
[8] T. Sakamoto, T. Kawamura, and G. Hashiguchi, Appl. Phys. Lett. **23**, 1612 (1986).
[9] P. I. Cohen, G. S. Petrich, P. R. Pukite, G. J. Whaley, and A. S. Arrot, Surf. Sci. **216**, 222 (1989).
[10] L.-M. Peng and H. J. Whelan, Surf. Sci. Lett. **238**, L446 (1990).
[11] T. Kawamura, Surf. Sci. **298**, 331 (1993).
[12] Y. Horio and A. Ichimiya, Ultramicroscopy **55**, 321 (1994).
[13] Y. Horio and A. Ichimiya, Surf. Sci. **133**, 393 (1983).
[14] A. Ichimiya, *The Structure of Surfaces III*, Springer Series in Surface Sciences Vol. 24 (Springer, Berlin, 1991), p. 162.
[15] Y. Horio and A. Ichimiya, Physica B **117/118**, 792 (1983).
[16] A. Ichimiya and Y. Takeuchi, Surf. Sci. **128**, 343 (1983).
[17] Y. Horio and A. Ichimiya, Surf. Sci. **164**, 589 (1985).
[18] G. Meyer-Ehmsen, *Reflection High-Energy Electron Diffraction and Reflection Electron Imaging of Surfaces*, Vol. 188 of *NATO Advanced Studies Institute Series B: Physics*, edited by P. K. Larsen and P. J. Dobson (Plenum, New York, 1988), p. 99.
[19] H. Marten, in *Reflection High-Energy Electron Diffraction and Reflection Electron Imaging of Surfaces* (Ref. 18), p. 109.
[20] H. Nakayama, T. Nishino, K. Ueda, S. Takeno, and H. Fujita, Ultramicroscopy **39**, 329 (1991).
[21] P. B. Swell and M. Cohen, Appl. Phys. Lett. **11**, 298 (1967).
[22] S. Miyake, K. Hayakawa and R. Miida, Acta Crystallogr., Sect. A: Cryst. Phys., Diffr., Theor. Gen. Crystallogr. **24**, 182 (1968).
[23] D. F. Mitchell, P. B. Swell, and M. Cohen, Surf. Sci. **69**, 310 (1977).
[24] S. Hasegawa, S. Ino, Y. Yamamoto, and H. Daimon, Jpn. J. Appl. Phys., Part 2 **24**, L387 (1985).
[25] J. C. H. Spence and Y. Kim, in *Reflection High-Energy Electron Diffraction and Reflection Electron Imaging of Surfaces*, (Ref. 18), p. 117.
[26] Y. Horio, Jpn. J. Appl. Phys., Part 1 **35**, 3559 (1996).
[27] Y. Horio and A. Ichimiya, Surf. Sci. **348**, 344 (1996).
[28] A. Ichimiya, Jpn. J. Appl. Phys., Part 1 **22**, 176 (1983); **24**, 1365 (1985).
[29] P. A. Doyle and P. S. Turner, Acta Crystallogr., Sect. A: Cryst. Phys., Diffr., Theor. Gen. Crystallogr. **24**, 390 (1968).
[30] S. L. Dudarev, L.-M. Peng, and M. J. Whelan, Surf. Sci. **330**, 86 (1995).
[31] S. Miyake and K. Hayakawa, Acta Crystallogr., Sect. A: Cryst. Phys., Diffr., Theor. Gen. Crystallogr. **26**, 60 (1970).
[32] A. Ichimiya, K. Kambe, and G. Lehmpfuhl, Jpn. J. Appl. Phys., Part 1 **49**, 684 (1980).
[33] H. Marten and G. Meyer-Ehmsen, Surf. Sci. **151**, 570 (1985).
[34] S. L. Dudarev and M. J. Whelan, Int. J. Mod. Phys. B **10**, 133 (1996).
[35] S. L. Dudarev and M. J. Whelan, Acta Crystallogr., Sect. A: Cryst. Phys., Diffr., Theor. Gen. Crystallogr. **53**, 63 (1997).
[36] P. A. Maksym and J. L. Beeby, Appl. Surf. Sci. **11/12**, 663 (1982).
[37] L.-M. Peng and J. M. Cowley, Acta Crystallogr., Sect. A: Cryst. Phys., Diffr., Theor. Gen. Crystallogr. **42**, 545 (1986).
[38] Y. Horio, Jpn, J. Appl. Phys. (to be published).